Physical properties of Cu nanoparticles: A molecular dynamics study

ARTICLE *in* MATERIALS CHEMISTRY AND PHYSICS · SEPTEMBER 2014

Impact Factor: 2.26 · DOI: 10.1016/j.matchemphys.2014.04.030

4 AUTHORS, INCLUDING:

Hasan Hüseyin Kart
Pamukkale University
27 PUBLICATIONS **194** CITATIONS
SEE PROFILE

S. Özdemir Kart
Pamukkale University
18 PUBLICATIONS **188** CITATIONS
SEE PROFILE

Tcagin Cagin
Texas A&M University
218 PUBLICATIONS **4,695** CITATIONS
SEE PROFILE

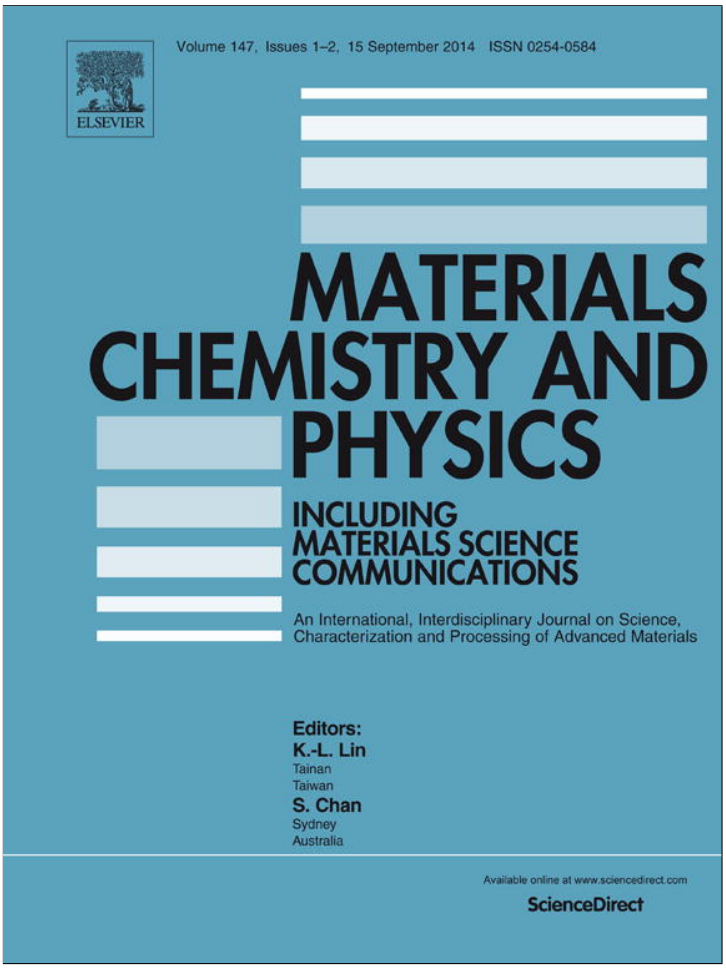

Materials Chemistry and Physics 147 (2014) 204–212

Contents lists available at ScienceDirect

Materials Chemistry and Physics

journal homepage: www.elsevier.com/locate/matchemphys

Physical properties of Cu nanoparticles: A molecular dynamics study

H.H. Kart [a,*], H. Yildirim [a], S. Ozdemir Kart [a], T. Çağin [b,c]

[a] Department of Physics, Pamukkale University, Kınıklı Campus, 20017 Denizli, Turkey
[b] Department of Materials Science and Engineering, Texas A&M University, College Station, TX 77845-3003, USA
[c] Department of Chemical Engineering, Texas A&M University, College Station, TX 77845-3122, USA

HIGHLIGHTS

- Solid and liquid properties of Cu nanoparticles are studied.
- Molecular dynamics utilizing the Quantum Sutton Chen potential is used in this work.
- Melting temperatures of nanoparticles are strongly depended on nanoparticle sizes.
- Heat capacity, radial distribution function and diffusion coefficients are studied.
- Structures of nanoparticles are analyzed by Lindemann and Honeycutt–Andersen index.

ARTICLE INFO

Article history:
Received 6 August 2013
Received in revised form
7 April 2014
Accepted 19 April 2014

Keywords:
A. Nanostructures
C. Molecular dynamics
D. Thermodynamic properties
D. Diffusion

ABSTRACT

Thermodynamical, structural and dynamical properties of Cu nanoparticles are investigated by using Molecular Dynamics (MD) simulations at various temperatures. In this work, MD simulations of the Cu-nanoparticles are performed by means of the MPiSiM codes by utilizing from Quantum Sutton-Chen (Q-SC) many-body force potential to define the interactions between the Cu atoms. The diameters of the copper nanoparticles are varied from 2 nm to 10 nm. MD simulations of Cu nanoparticles are carried out at low and high temperatures to study solid and liquid properties of Cu nanoparticles. Simulation results such as melting point, radial distribution function are compared with the available experimental bulk results. Radial distribution function, mean square displacement, diffusion coefficient, Lindemann index and Honeycutt–Andersen index are also calculated for estimating the melting point of the Copper nanoparticles.

1. Introduction

Nanoscience and nanotechnology are concerned with the manipulation of matter on the nanometer length scale, which is considered as the 1–100 nm range. Especially, nanoparticles are of great scientific interest as they are effectively a bridge between the bulk materials and atomic and molecular structures [1]. Clusters and nanoparticles are aggregates of between a few and many millions of atoms or molecules. Interest in the nanoparticles arises because they form a new type of material, which may have properties which are distinct from those of individual atoms and molecules or bulk matter. Therefore, many nanostructured materials have shown exciting properties and applications [2,3]. Recently, considerable attention has been paid to nanosize coinage metal clusters, which are of great importance in fabricating nano electronic devices, and novel nano-catalysis as mentioned in the Ref. [4]. In the past decades, much attention has been paid to the studies of the thermal structure and melting behavior of metal clusters as seen in Ref. [5]. An important reason for the interest in metal nanoparticles is due to the size dependent evolution of their physical, chemical, and electronic properties [6–9].

The thermodynamical properties of nanoparticles during the phase transition have been widely studied and these properties are different from those of the bulk system due to the size effect. The investigation of this kind of phase transition leads to the understanding of thermodynamics of finite systems [10–12].

Transition metals and their alloys are very important both scientifically and technologically [13,14]. Recently, considerable attention has been paid to copper metal nanoparticles in the past two decades because of their unusual properties and potential applications in many fields as mentioned in Refs. [15,16]. For example, non-agglomerated, spherical, uniform copper nanoparticles are desired for conductive films, lubrication, nanofluids

* Corresponding author.
E-mail addresses: hkart@pau.edu.tr, hhkart2001@gmail.com (H.H. Kart).

http://dx.doi.org/10.1016/j.matchemphys.2014.04.030
0254-0584/

and etc. Copper (Cu) nanoparticles are also widely used as an algaecide, fungicide, interconnection of computers, nanorods and nanodisks. Additionally, Cu nanoparticles have many advantages such as economic, lightweight and formable [17]. This metal has also found potential applications in the future industrial applications in the area of microelectronics, heat transfer systems, gas separations and storage-hydrogen, and super strong materials. Therefore it is important to understand the properties of Cu nanoparticles to develop new materials based on ones.

In general, the nanoparticles are modeled in the hope of understanding their physical properties in terms of their structures and sizes. The main aim of modeling of the nanoparticles is to be able to undertake virtual experiments, serving as a complement to conventional experiments, allow us to learn the new information about it, or something that cannot be found out in other ways. One advantage of the modeling of the nanoparticles over conventional ways is that it allows ones to understand and comprehend a path through the complexity inherent in the nanoscience and nanotechnology.

Atomistic simulations techniques such as molecular dynamics (MD) have become a powerful tool in the field of nanotechnology as they provide a physical insight in understanding various phenomena at atomic scale and enable one to predict the physical properties such as structure and thermodynamics properties of the nanomaterial. It is expected that atomistic simulation has an important role in complementing experiments in the study of nanomaterial, since the experimental studies of the nanomaterial encounter many technical difficulties.

In the last years, many researchers have studied the structure, thermodynamics, and liquid properties of metal nanoparticles [18–23]. For example, Lewis et al. presented a detailed molecular dynamics study of the melting, freezing, and coalescence of gold nanoclusters within the framework of the embedded-atom method [24]. They show that melting process first affects the surface, and then it proceeds inward region of the nanoparticles. Qi et al. investigated the melting and freezing of Ni nanoclusters with up to 8007 atoms (5.7 nm) by using the molecular dynamics with the quantum-Sutton-Chen many-body force field [25]. Zhang and Sun studied the structural changes of the three Cu clusters containing 51–53 atoms during their melting processes by using the molecular dynamics simulation utilizing EAM [26]. Moreover, Zhang and Fan have used the molecular dynamics simulation method with the embedded atom potential (EAM) to investigate the structural change of a molten Cu_{411} clusters during quenching [27]. They have shown that quenching temperature strongly affects locally ordered structural changes. Atomistic simulations on the nanoparticles having a great number of atoms in the literature are scarce. Therefore, much more computations on the large sizes of nanoparticles are needed to understand the structural, thermodynamics, dynamics and melting properties of them.

In this paper, we have applied the MD method utilizing the Quantum Sutton Chen (Q-SC) many body force field to investigate the solid, liquid and melting properties of Cu nanoparticles containing from 369 atoms to 44,403 atoms. Diameters of the nanoparticles considered in this work are changed from 2 nm to 10 nm. In particularly, we have analyzed that how the melting temperature, heat capacity, radial distribution function, mean square displacement, diffusion coefficient, Lindemann index and Honeycutt–Andersen index of nanoparticles are depend on nanoparticle sizes, including pre-melting of the nanoparticles to estimate the phase transition from solid to liquid.

This paper is organized as follows: In Section 2, we briefly describe the computational method and simulation procedure. Section 3 deals with the simulation results of Cu nanoparticles when the continuous heating processes are applied to the Cu nanoparticles at low and high temperatures. The detailed discussion on their structural evolution and comparison with bulk results are also presented in the same section. Finally, the main conclusions arising from this work are summarized in Section 4.

2. Computational method

In this work, we have used the molecular dynamics (MD) simulations method in the TVN ensemble to elucidate the structure and thermodynamic properties of various sized nanoparticles whose diameters are changed from 2 nm to 10 nm. This method is very suitable for modeling of large systems for the long time scales. Modern ab initio methods are not yet feasible to study large systems for the long time scales. MD simulations [28–30] are performed by means of the MPiSiM software developed at Caltech [31]. This program uses the quantum corrected Sutton-Chen (Q-SC) many-body force field [32–34]. The modified Sutton-Chen potential was empirically fitted to data on density, cohesive energy, compressibility, and phonon frequency. Q-SC produces accurate values for surface energy, vacancy energy, and stacking fault energies and has been used in the studies of melting, glass formation and crystallization of pure metals, and their alloys and nanoparticle [31,35,36]. In our previous study [37], we have used Q-SC potential to study the coalescence of equal and unequal sized Cu nanoparticles at low and high temperatures.

Five different model systems of the spherical Cu nanoparticles are generated to start the molecular dynamics simulation of the Cu nanoparticles. Fig. 1 shows the five different sized initial structures of the spherical Cu nanoparticles. The models with spherical nanoparticles are inserted into a rectangular box which has the dimensions of 200 Å, 200 Å, 200 Å, in the x, y and z directions, respectively. All models considered in this work are equilibrated by using MPiSiM program at elevated temperatures ranging from 100 K to 1500 K by increasing temperature of 100 K. The increment of the temperature around the melting temperatures of the nanoparticles is taken as the 20 K to better estimate the melting points of nanoparticles.

The spherical nanoparticles model systems are equilibrated over 50,000 time steps in the constant-volume, constant-temperature ensemble (TVN) at the target temperature. Molecular dynamics time step is set as 2 fs.

Quantum Sutton-Chen (QSC) many-body potential is used to define the interaction between the Cu atoms. Total potential energy of the transition metals and their alloys in the Sutton-Chen formalism for the system of N atoms is given as follows [33–36];

$$U_{\mathrm{tot}} = \sum_i U_i = \sum_i \left[\frac{1}{2} \sum_{j \neq i} \varepsilon \left(\frac{a}{r_{ij}} \right)^n - c\varepsilon \left(\sum_{j \neq i} \left(\frac{a}{r_{ij}} \right)^m \right)^{1/2} \right] \quad (1)$$

The first term in the Eq. (1) is a two body repulsive interaction between the atoms i and j, separated by a distance r_{ij}. The second term represents the many-body cohesion term associated with atom i. The square root term introduces a many-body component into the energy summation. The popularity of SC potentials is partly due to the computationally tractable form adopted for the many-body forces. It is the relatively simple analytic form of the potential that enables one to calculate the many physical properties of some face centered cubic (fcc) metallic materials.

In the Eq. (1), r_{ij} is the distance between atoms i and j, a is a length parameter scaling to the lattice spacing of the crystal, c is a dimensionless parameter scaling the attractive terms, ε is an energy parameter determined from experiment, and n, m are integer parameters with $n > m$ which determine the range of the two components of the potential. The interaction length of potential is taken

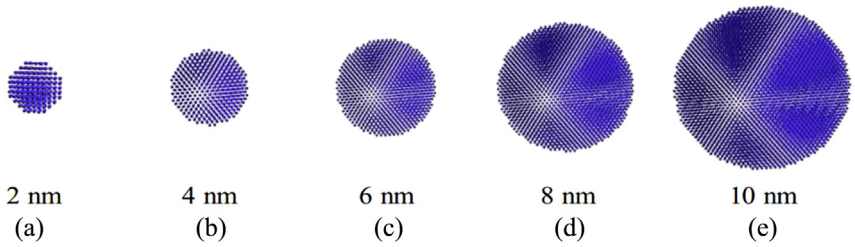

Fig. 1. Initial structures 2 nm (a), 4 nm (b), 6 nm (c), 8 nm (d) and 10 nm (e) of the spherical nanoparticles with diameters of various sizes from 2 nm to 10 nm with increment of 2 nm, respectively.

as two lattice parameters for the efficiency of the computer simulation time. The temperature effects in the simulations are considered by giving an additional length of half of the lattice parameter.

The Q-SC potential parameters for the Cu are given in Table 1 [32,37].

3. Results and discussions

To understand the thermodynamics, structural and dynamical properties of the different sizes of copper nanoparticles we have presented some results such as melting points, heat capacity, radial distribution function, first coordination number, Honeycutt–Andersen index and Lindemann index, mean square displacement and diffusion coefficient of them.

3.1. Melting point

The melting point of a solid is the temperature at which it changes from solid state to liquid one. At the melting point, the solid and liquid phases coexist in the equilibrium. Thus melting of a material is a characteristic of a substance and can be used to identity it [38]. The method used for predicting the melting transition is the calculation of the caloric curve (total energy (TE) per atom versus temperature graph) by heating the nanoparticles from a low temperature solid configuration to a high melted state as shown in Fig. 2(a). TE of the nanoparticles increases while the temperature of them increases up to melting region. There are sharp jumps around the melting temperature of the nanoparticles, corresponding to a sharp peak in the heat capacity as shown in Fig. 2(b), (c) and (d). The multiple peaks in the heat capacity curve can be observed in the graphs of small nanoparticles as mentioned in Ref. [39]. These peaks are associated with a changing of the structure of the nanoparticles [39]. In addition, we have also investigated some physical properties of the nanoparticles such as radial distribution function, mean square displacement and diffusion coefficient to exactly predict the melting point of the different sized of Cu nanoparticles.

Simulation results can be compared with the available experimental results of bulk Cu metal since the physical properties of nanoparticles are not available in literature. We have fitted the melting point values of nanoparticles studied in this work to an equation to estimate the melting values of the other sizes of the Cu nanoparticles as shown in Fig. 3. The melting temperature of nanoparticles can be represented by the following equation [40];

Table 1
Q-SC potential parameters for Cu metal.

n	m	ε(eV)	c	$a(\mathring{A})$
10	5	5.7921E-3	84.8430	3.6030

$$1-\frac{T_{cm}}{T_{CM}}=\frac{z\beta}{D-2\delta}, \tag{2}$$

where, T_{cm} is the melting temperature of nanoparticle studied in this work, T_{CM} is the bulk melting temperature, D is the diameter of nanoparticles, $\beta = 2V/\Delta H_f(\gamma_{sv}-\gamma_{lv})$, ΔH_f is the bulk latent heat of fusion, γ_s is surface energies of solid–vapor and liquid–vapor interfaces of the material and $z=3$ for liquid skin melting. The δ value is positive only for liquid skin melting.

As shown in Fig. 2(a)–(d), the melting points of Cu nanoparticles become bigger while the sizes of nanoparticles increase. The predicted melting points of the nanoparticles and the curve according to the Eq. (2) are consistent with each other. This allows ones to predict the melting points of other size nanoparticles.

MD method is also used to find the melting temperature of the bulk Cu via quantum Sutton-Chen potential. It is predicted as 1358 K, which is very close to the experimental value of T_m, 1356 K, for bulk Cu.

3.2. Heat capacity

The specific heat capacity can be obtained from the ensemble averages of the potential energy (PE) and its square, such as [41];

$$\frac{C}{k_B}=\frac{1}{Nk_B^2T^2}\left(\left\langle PE^2\right\rangle-\langle PE\rangle^2\right)+\frac{3}{2}. \tag{3}$$

In the Eq. (3), the first term is the average potential energy and the second term is kinetic energy contribution for the canonical ensemble. N is the number of particles in the model systems, k_B is Boltzmann constant, and T is the temperature.

Fig. 2(b), (c) and (d) show the behavior of the heat capacity with respect to temperature for the nanoparticles with the diameters of 2 nm, 4 nm and 6 nm, respectively. There are sharp peaks around the melting temperatures of the Cu nanoparticles as seen in Fig. 2(b)–(d). These peaks represent the phase transition temperature from solid phase to liquid one. These sharp peaks are observed at higher temperatures with increasing size of Cu nanoparticles. These changes in the nanoparticles are consistent with the behavior of total energy as a function of temperature as shown in Fig. 2(a).

3.3. Radial distribution function

Radial distribution function (RDF) is very important tool to determine the structural properties of materials. In the systems consisting of a single type of atom, RDF is defined as follows [42–44];

$$g(r)=\frac{V}{N}\frac{n(r)}{4\pi r^2\Delta r}. \tag{4}$$

In the Eq. (4), V is the volume of the system, N is the number of particle in the system, $n(r)$ is number of atoms in the thickness of Δr

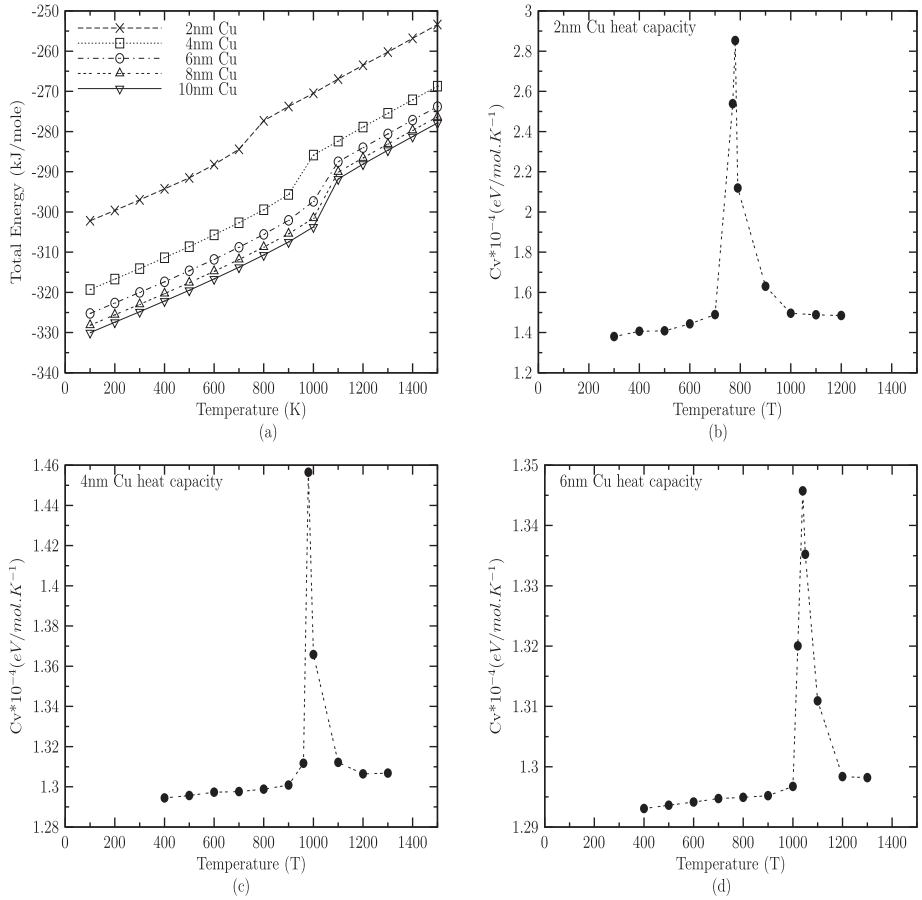

Fig. 2. (a) Behavior of total energy as a function of temperature according to the size of nanoparticles. Temperature dependence of the heat capacity for Cu nanoparticles with the diameters of (b) 2 nm (c) 4 nm (d) 6 nm, respectively.

at the radius (r) of the nanoparticle. RDF is a measurement of an average probability of finding a particle at a distance of r away from a given reference particle.

Radial distribution functions of the different sizes of the nanoparticles are plotted in Fig. 4(a)–(g) at elevated temperatures to examine the structural behavior of them. Fig. 4(a) is given to show the behavior of RDF of the 2 nm nanoparticle at the temperatures of 300 K, 700 K, 1000 K and 1200 K, respectively. Fig. 4(b) is also plotted to compare the behavior of RDF of the bulk Cu material and Cu nanomaterial with the size of 2 nm as given in Fig. 4(a). The behaviors of RDF for the different sizes of Cu nanomaterial are given in Fig. 4(c)–(g) at elevated temperatures. RDF graphs have a number of important features. Firstly, as shown in the graphs of Fig. 4, the RDF is zero at short distances (small r), indicating the effective width of the atoms. This is due to the fact that they cannot approach any more closely each other. Secondly, a number of obvious peaks indicate that the atoms are sited down around each other in shells of neighbors. Thirdly, the peaks of the radial distribution function before the melting temperature are usually sharp at low temperature. This is due to fact that the atoms are closely located around the each other. The peaks are broad at higher temperature, indicating thermal motion. The atoms begin freely to move away from lattice point. Fourthly, the third and fourth peaks in RDF observed at low temperatures have disappeared when with increasing temperature (at 1200 K), which represent a liquid like behavior of the nanoparticles. Graphs in Fig. 4 show that RDF converges to one with increasing temperature. Interaction between the atoms in the liquid state is lost, thus, the central atom goes far away distant with increasing temperature. Finally, the second peak in RDF disappears after the melting point and then width of the first peak of RDF decreases. It is concluded that the peaks of the RDF for the bulk Cu are generally the most sharpest than them of the nanoparticles at elevated temperatures.

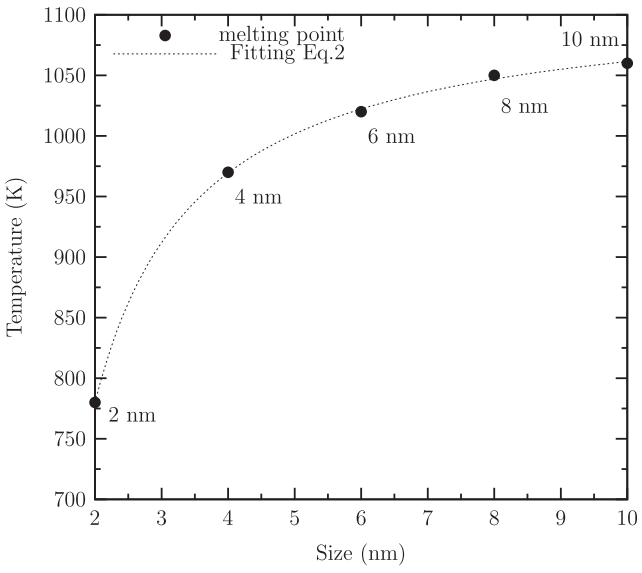

Fig. 3. Dependence of melting point on cluster size.

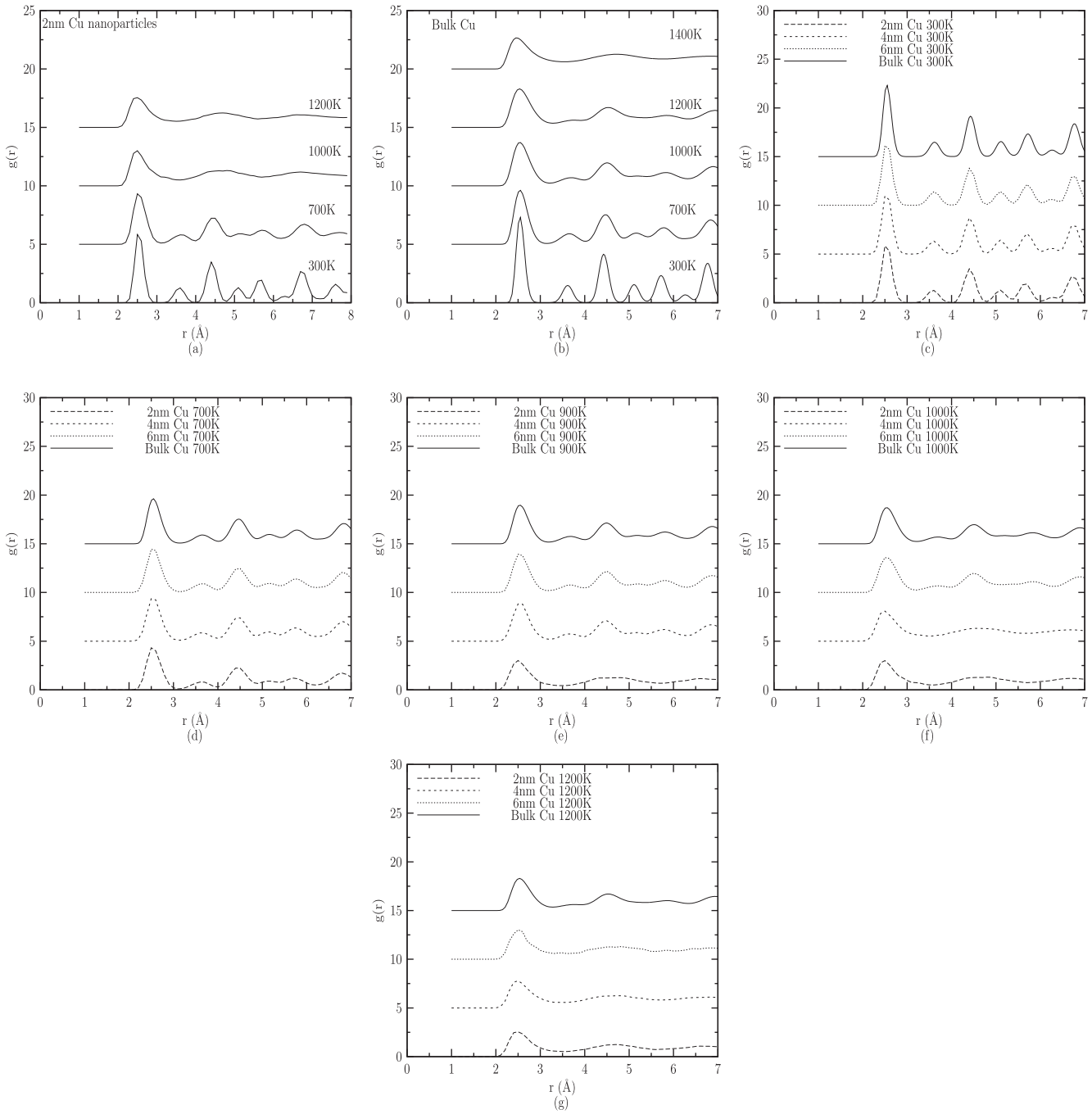

Fig. 4. Behavior of radial distributions functions for the different sizes of copper nanoparticles at various temperatures (a) 2 nm, (b) bulk Cu, and comparison of different sizes of nanoparticles with the bulk copper at (c) 300 K, (d) 700 K, (e) 900 K, (f) 1000 K, and (g) 1200 K.

3.4. First coordination number

The area of first maximum peak of radial distribution function graphs is used to calculate the number of first nearest neighbor atoms in the nanoparticles. It is defined as follows [45];

$$Z = 4\pi\rho \int_0^{r_c} r^2 g(r)\mathrm{d}r, \tag{5}$$

where, ρ is the atomic number density and r_c is the position of the first minimum in $g(r)$. The integral on the right side of this formula is calculated by using the Simpson's rule [46,47].

The transition metal copper atoms are arranged in fcc structure. The first coordination number of fcc structure for the copper is 12 in the solid state. As shown in the graph of Fig. 5, the first coordination number is very close to 12 until the temperature of the nanoparticle approaches to the melting point. It can be said that the first coordination number takes the same value until the melting points of the nanoparticles. In addition, the first coordination number decreases with increasing temperature after the melting point of nanoparticles. Although positions of atoms are definite in solid structure, these positions are indefinite in liquid structures. Additionally, Fig. 5 shows that the melting point of copper nanoparticles starts when the first coordination number begins to decrease sharply. The melting points of the nanoparticles estimated from

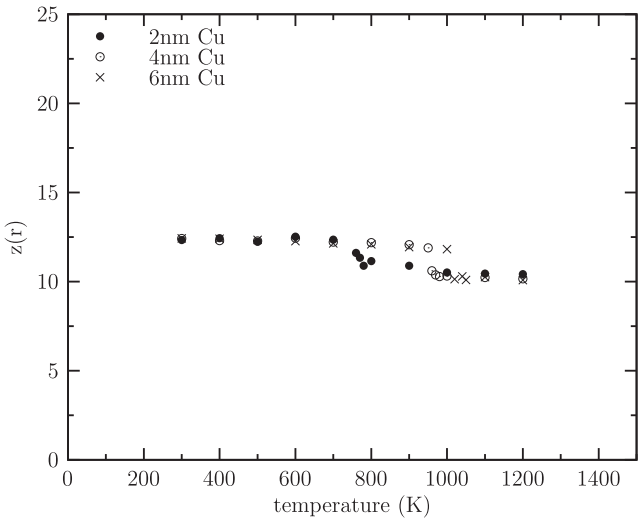

Fig. 5. Behavior of the first coordination number as a function of temperatures for 2 nm, 4 nm, and 6 nm Cu nanoparticles.

Fig. 4 are compatible with the values of them predicted from Fig. 2.

3.5. Honeycutt–Andersen index

The local geometric structure can be investigated by searching for local face centered cubic (fcc) structural regions in the copper nanoparticles by finding neighboring atoms with the fcc packing sequence. Among the methods which are mostly used for the structural analysis, the Honeycutt–Andersen index proposed by Honeycutt–Andersen (HA) is based on the nearest neighbor atoms [48,49]. HA method could describe the structural transition in small clusters with increasing size from icosahedral structure and poly-icosahedral to fcc [48]. Starting with a pair of atoms, α and β, the diagram is classified by a set of four indexes ($ijkl$) [48–52]: where; (i) with values of 1 or 2 indicates that α and β are nearest neighbors ($i = 1$) or not ($i = 2$); (j) indicates the number of nearest neighbors shared by the (α, β) pair (common neighbors); (k) indicates the number of bonds among the common neighbors; (l) differentiates diagrams with some (i), (j), and (k) indexes and different bonding among common neighbors.

Two atoms are nearest neighbors if the distance between them is less or equal to a cut off distance, which is in general defined as the first minimum in the radial distribution function.

Fig. 6 is visualized by using the OVITO programme [53]. It shows the increment of the deformations in the nanoparticle with 2 nm diameter when the temperature of it increases. As shown in Fig. 6, the structure of nanoparticle becomes the disordered at the higher temperatures of 300 K. The number of atoms of nanoparticle in the fcc structure decreases with the increasing temperature as seen in Fig. 6. This is due to the fact that atoms move away from each other as the temperature increases and then crystal structure of nanoparticle starts to become disordered. The copper nanoparticle is not found in the fcc structure at 1000 K, that is, it is completely melted after this temperature.

3.6. Lindemann index

The Lindemann index has been commonly used to define the melting transition of nanoparticles. The root-mean-square (rms) bond fluctuation called Lindemann index δ has been often used to discuss the phase transition temperature. The Lindemann index is defined as [10,54];

$$\delta = \frac{2}{N(N-1)} \sum_{i<j} \frac{\sqrt{\left\langle r_{ij}^2 \right\rangle - \left\langle r_{ij} \right\rangle^2}}{\left\langle r_{ij} \right\rangle}, \tag{6}$$

here, r_{ij} is the distance between atoms i and j, N is the number of atoms in the particle, and the brackets $\langle\rangle$ represent the ensemble average at the temperature of the sample. Additionally, Lindemann index is important tool to examine the sample in the layer form in order to determine the melting which is beginning in inner region or outer region of the model systems. Lindemann index of each layer is expressed as [55];

$$\delta_{L(i)} = \frac{2}{N_{L(i)}\left(N_{L(i)} - 1\right)} \sum_{j<k} \frac{\sqrt{\left\langle r_{jk}^2 \right\rangle - \left\langle r_{jk} \right\rangle^2}}{\left\langle r_{jk} \right\rangle}, \tag{7}$$

where, $L(i)$ is the ith layer and $N_{L(i)}$ is number of atoms of the ith layer, r_{jk} is the separation distance between the atom j and k.

Fig. 7(a) shows the temperature dependence of the Lindemann index of the 2 nm Cu nanoparticle. If we look at the behavior of the Lindemann index as a function of temperature as shown in Fig. 7(a), it is evident that the melting point of the nanoparticle is around the 780 K. It is also clear from the figure that the melting process can be divided into three stages. In the first stage, where the temperature is lower than 500 K, the Lindemann index increases slowly and linearly with temperature. During the second stage (500 – 780 K) the increase in the Lindemann index is rapid (compared to the first stage) and non-linear. The third stage is the high temperature region where the nanoparticle is completely melted and the value of Lindemann index reaches a maximum of about 0.375.

The linear increasing of the Lindemann index during the first stage is due to the increasing of the atomic kinetic energy with temperature. The value of the Lindemann index during this stage is very small since most of the nanoparticle atoms, including those in the central part and on the surface, do not have large amplitude motion but they merely vibrate around their original lattice positions. That is, the nanoparticle is solid state at these temperatures.

The behaviors of the Lindemann index of each layer for 2 nm Cu nanoparticle with respect to temperature are given in Fig. 7(b) to comprehend the melting mechanism with respect to layers. As shown in Fig. 7(b), the atoms on the surface of the nanoparticle

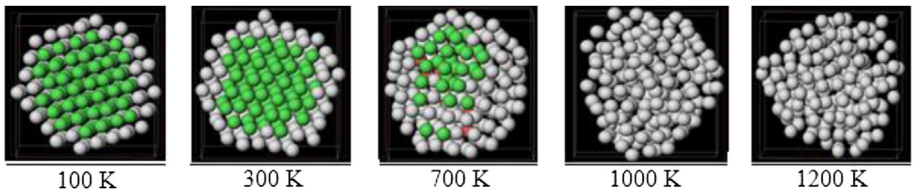

Fig. 6. Snapshots of the Honeycutt–Andersen index of 2 nm Cu nanoparticle at various temperatures. Green atoms indicate the fcc structure while red atoms represent hcp structure. (For interpretation of the references to colour in this figure legend, the reader is referred to the web version of this article.)

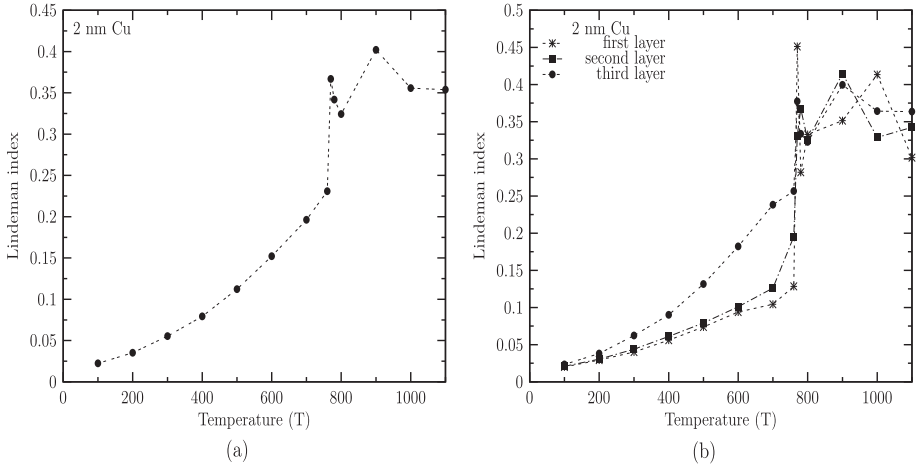

Fig. 7. (a) Lindemann index as a function of temperature during the heating processes of 2 nm Cu nanoparticle. (b) Behavior of the layered Lindemann index for the 2 nm, 4 nm and 6 nm Cu nanoparticles with respect to temperature.

have large Lindemann index than those of them near the center of it, which confirms the fact that the surface atoms have large diffusion amplitude from their original lattice positions while the central atoms of nanoparticle remain their original lattice positions. It is also evident that an increase in temperature leads to an increase in the number of surface atoms that diffuse from their lattice positions, i.e., an increase in temperature gives rise to an increment of the surface diffusion or surface melting of the nanoparticles.

3.7. Mean square displacement and diffusion coefficient

In order to analyze the atomic motions before and after the melting point of the model systems, we have used mean square displacement (MSD). MSD is a measure of the average distance that a given particle in a system travels. The MSD is defined as [20,56–58];

$$\mathrm{MSD} = \left\langle r^2(t) \right\rangle = \left\langle \frac{1}{N}\sum_{i=0}^{N} (r_i(t) - r_i(0))^2 \right\rangle. \quad (8)$$

Here, N is the number of particles, t corresponds to time, and $r_i(t) - r_i(0)$ is the vector distance traveled by a given particle over the time interval. If the particle travels ballistically, the distance traveled by the particles is proportional to the time interval. Therefore, MSD increases as a quadratic. In the dense phases of the materials, the ballistic motion only takes place for very short time scales. After the ballistic regime, the MSD will increase linearly with time. The plot of the mean square displacements for the copper nanoparticle with 2 nm diameter are given in Fig. 8. The behavior of the mean square displacement is not linear at very short times as seen in Fig. 8 before the melting temperature. This is due to the fact that the path of a molecule takes will be an approximate straight line until it collides with its neighbor. Until it makes the first collision with its neighbor, we may say that it moves with approximately constant velocity, which means the distance it travels is proportional to time, and its MSD is therefore proportional to time squared. Thus, MSD resembles a parabola at very short times. The MSD provides the important information about the atomic diffusion. The temperature dependent diffusion coefficients have been calculated from the slope of the curves as shown in Fig. 8 according to Eq. (9). Undoubtedly, the gradually increased slopes of the curves suggest that the diffusivity increases with temperature. This is due to the fact that collision frequency between atoms accelerates with an increasing temperature, resulting in the increase in the MSD of the atoms.

Dynamical properties of the materials are the important physical quantities of the liquid systems to understand the detailed atomistic mechanism of diffusive motion. The diffusion coefficient can be computed from the slope of the MSD at long time intervals.

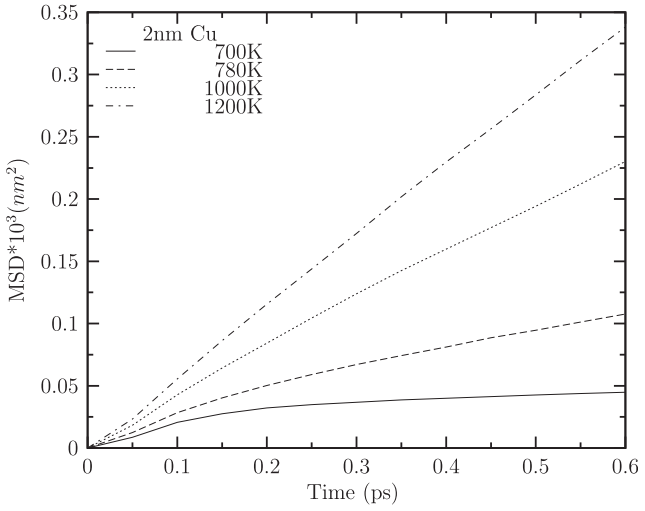

Fig. 8. The behavior of the MSD with respect to time for Cu nanoparticles with the diameter of 2 nm at different temperatures.

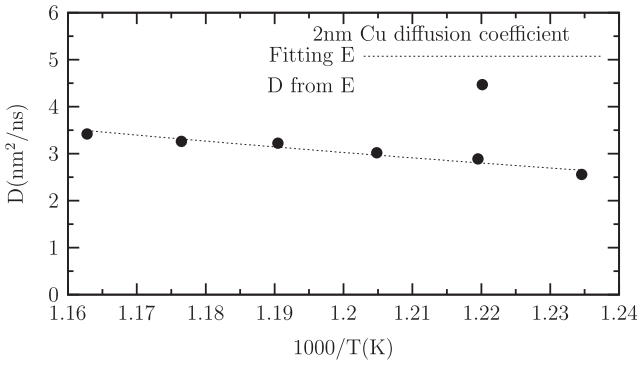

Fig. 9. Behavior of Arrhenius equation as a function of temperature, fitted to data of the diffusion coefficient D computed from Einstein (E) relations for the nanoparticle having diameter of 2 nm.

Table 2
The values of the diffusion coefficients D(nm^2 ns^{-1}), the pre-exponential factor D_0(nm^2 ns^{-1}) and the activation energy E_a(eV) for the various sized nanoparticles at elevated temperatures.

Size of nanoparticles (nm)	D_0 (nm^2 ns^{-1})	E_a (eV)	D (300 K) (nm^2 ns^{-1})	D (800 K) (nm^2 ns^{-1})	D (1000 K) (nm^2 ns^{-1})	D (1200 K) (nm^2 ns^{-1})
2	306.4	0.0310824	2.964×10^{-5}	2.937	4.876	6.617
4	306.4	0.0310115	9.313×10^{-2}	0.537	7.631	13.511
6	306.4	0.0310143	5.854×10^{-2}	0.304	1.806	14.451

The Einstein formula is used to calculate the diffusion coefficient D given as [56,59];

$$D = \frac{1}{6}\lim_{t\to\infty}\frac{\mathrm{d}}{\mathrm{d}t}(\mathrm{MSD}). \quad (9)$$

In order to compute the necessary activation energy for diffusion, we have used the Arrhenius equation given as follows [60,61];

$$D(T) = D_0 \exp\left(-\frac{E_d}{k_B T}\right), \quad (10)$$

where, D_0 is the pre-factor of Arrhenius equation, k_B is the Boltzmann constant, T is temperature, and E_d is the diffusional activation energy. Arrhenius function fitted to data of the diffusion coefficient D computed from the Einstein (E) relation is given in Fig. 9 for the nanoparticle with the diameter of 2 nm. Logarithmic representation of the diffusion coefficients has been plotted by using the Arrhenius type equation, as given in Fig. 9, as a function of 1000/T temperature. The dashed line in Fig. 9 represents an Arrhenius fitting curve through data points evaluated from Einstein relation as given in Eq. (9). As shown in Fig. 9, the values of diffusion coefficients computed by using the Einstein relations and Arrhenius fit at various temperatures are mutually consistent.

We have also predicted the melting temperatures of the nanoparticles by checking the values of diffusion coefficient. The diffusivities of the order of 10^{-3} nm^2 ps^{-1} (see in Table 2) help us to distinguish the liquid state from the solid state [62]. The self-diffusion coefficient data of the various sized nanoparticles calculated from Arrhenius equation at different temperatures are given in Table 2. The value of the self-diffusion coefficient for the 2 nm nanoparticle at 800 K is greater than the values of the other sized nanoparticles. This is expected result because small nanoparticle starts to melt early temperature than other nanoparticles with the diameters having 4 nm and 6 nm.

4. Conclusions

The molecular dynamics simulation results by using the Q-SC many-body potential for the physical properties of different sizes of Cu nanoparticles are presented at various temperatures for the first time in this study. The simulation results are in good agreement with the available experimental data. One of the achievements of this work is to predict the melting temperatures of Cu nanoparticles by analyzing the physical properties calculated in this work. Melting temperatures of the copper nanoparticles is found to be increased as the size of the nanoparticles increases as we expected. In addition, the behavior of the radial distribution function of the copper nanoparticles is found to be consistent with the other studies and values of the bulk. Honeycutt–Andersen index shows that the numbers of fcc atoms are found to be decreased with increasing temperature. Diffusion coefficients calculated by using the slope of MSD curve are found to be fitted to the Arrhenius curve. It is also shown from the Lindemann index that an increase in the temperature of the nanoparticles gives rise to an increment of the number of surface atoms that diffuse from their lattice positions, i.e., an increase in temperature leads to an increment of the surface diffusion or surface melting of the nanoparticles.

Molecular dynamics simulation results for the different sizes of nanoparticles provide us to understand the basics process of the melting driving mechanism. MD simulations allow ones to synthesize and develop a new functional nanostructured material by controlling the nanoparticles size and by increasing the number of nanoparticles to guide the experimentalists.

Q-SC potential parameters are able to reproduce the thermodynamics, structural and dynamical properties of different sizes of Cu nanoparticles at low and high temperature.

Acknowledgments

Calculations are carried out by using computer facilities of BAP projects (BAP Project No: 2010FBE076, 2010FBE083, 2011FBE077, and 2012FBE002) conducted in the Department of Physics supported by Pamukkale University. Moreover, Dr. Tahir Cagin is also financially supported by TUBITAK-BIDEB to give a final form to this work.

References

[1] G.A. Ozin, A.C. Arsenault, Nanochemistry: A Chemical Approach to Nanoparticles, RSC Publishing, Cambridge, 2005.
[2] R. Birringer, Mater. Sci. Eng. A 117 (1989) 33–43.
[3] P. Moriarty, Rep. Prog. Phys. 64 (2001) 297–381.
[4] Z. Lin, L. Wei, W.S. Qing, Chin. Phys. B 19 (2010) 073601.
[5] M.H. Ghatee, K. Shekoohi, Fluid Phase Equilibr. 327 (2012) 14–21.
[6] R. Ferrando, J. Jellinek, R. Johnston, Chem. Rev. 108 (2008) 845–910.
[7] R.L. Johnston, Atomic and Molecular Clusters, Taylor & Francis, 2002.
[8] P. Nayebi, E. Zaminpayma, J. Clust. Sci. 20 (2009) 661–670.
[9] Y. Wen, H. Fang, Z. Zhu, S. Sun, Phys. Lett. A 373 (2009) 272–276.
[10] Y. Shibuta, T. Suzuki, J. Chem. Phys. 129 (2008) 144102.
[11] W.H. Qi, B.Y. Huang, M.P. Wang, F.X. Liu, Z.M. Yin, Comput. Mater. Sci. 42 (2008) 517–524.
[12] W. Zhang, F. Zhang, Z. Zhu, Phys. Rev. B 74 (2006) 033412.
[13] H. Gleiter, Prog. Mater. Sci. 33 (1989) 223–315.
[14] G. Fracasso, Synthesis and Physical-chemical Characterization of Metallic Nanoparticles (Phd Thesis), University of Bologna, 2010.
[15] H. Zhu, C. Zhang, Y. Yin, Nanotechnology 16 (2005) 3079–3083.
[16] http://www.copper.org/applications/homepage.html.
[17] http://www.copper.org/publications/pub_list/pdf/copper_tube_handbook.pdf.
[18] Q. Chen, S.Y. Wang, M.H. Sun, Acta Phys. Sin.-Ch. Ed. 61 (2012) 308–314.
[19] X.Y. Yang, G.X. Tang, Int. J. Mod. Phys. B 26 (2012) 1250022.
[20] S.L. Gafner, L.V. Redel, Y.Y. Gafner, J. Exp. Theor. Phys. 14 (2012) 428–439.
[21] L.J. Meng, X.Y. Peng, K.W. Zhang, C. Tang, J.X. Zhong, J. Appl. Phys. 111 (2012) 024303.
[22] Y. Sang Chul, K. Da Hye, S. Kihyun, L. Hyuck Mo, Phys. Chem. Chem. Phys. 14 (2012) 2791–2796.
[23] N.P. Joshi, D.E. Spearot, B. Deepak, J. Nano. Nanotechnol. 10 (2010) 5587–5593.
[24] L.J. Lewis, P. Jensen, J.L. Barrat, Phys. Rev. B 56 (1997) 2248.
[25] Y. Qi, T. Çağın, W.L. Johnson, W.A. Goddard III, J. Chem. Phys. 115 (2001) 8061.
[26] L. Zhang, H. Sun, Phys. Status Solidi A 207 (2010) 1178–1182.
[27] L. Zhang, Q. Fan, Phys. Scr. 84 (2011) 045303.
[28] J. Ray, A. Rahman, J. Chem. Phys. 82 (1985) 4243.
[29] W.G. Hoover, Phys. Rev. A 31 (1985) 1695.
[30] M. Parrinello, A. Rahman, Phys. Rev. Lett. 45 (1980) 1196.
[31] Y. Qi, T. Cagin, W.A. Goddard III, J. Comput. Aided Mater. Des. 8 (2001) 185.
[32] T. Cagin, Y. Qi, H. Li, Y. Kimura, H. Ikeda, W.L. Johnson, W.A. Goddard III, MRS Symp. Ser. 554 (1999) 43.
[33] A.P. Sutton, J. Chen, Phil. Mag. Lett. 61 (1990) 139.
[34] H. Rafii-Tabar, A.P. Sutton, Phil. Mag. Lett. 63 (1991) 217.

[35] H.H. Kart, M. Tomak, T. Çağın, Model. Simul. Mater. Sci. Eng. 13 (2005) 657–669.
[36] H.H. Kart, M. Tomak, M. Uludoğan, T. Çağın, Comput. Mater. Sci. 32 (2004) 107.
[37] H.H. Kart, G. Wang, I. Karaman, T. Cagin, Int. J. Mod. Phys. C 20 (2009) 179–196.
[38] A.A. Shvartsburg, M.F. Jarrold, Phys. Rev. Lett. 85 (2000) 2530–2533.
[39] J.C.R. Gomez, L. Rincon, Rev. Mex. Fis. 53 (2007) 208–211.
[40] K.K. Nanda, Pramana-J. Phys. 72 (2009) 617–628.
[41] A. Bagrets, R. Werner, F. Evers, G. Schneider, D. Schooss, P. Wölfle, Phys. Rev. B 81 (2010) 075435.
[42] J.M. Haile, Molecular Dynamics Simulation: Elementary Methods, Wiley-Interscience, 1992.
[43] http://www.compsoc.man.ac.uk/~lucky/Democritus/Theory/rdf.html.
[44] http://matdl.org/matdlwiki/index.php/softmatter:Radial_Distribution_Function.
[45] D. Alfe, G. Kresse, M.J. Gillan, Phys. Rev. B 61 (2000) 61132–61142.
[46] J.F. Epperson, An Introduction to Numerical Methods and Analysis, Wiley-Interscience, 2007, pp. 261–272.
[47] L.A. Talman, Am. Math. Mon. 113 (2006) 144–155.
[48] J.D. Honeycutt, H.C. Andersen, J. Chem. Phys. 72 (1980) 2384–2393.
[49] H. Tsuzuki, P.S. Branicio, J.P. Rino, Comput. Phys. Commun. 177 (2007) 518–523.
[50] G. Zhang, Q. An, W.A. Goddard III, J. Phys. Chem. C 115 (2011) 2320–2331.
[51] T.H. Kim, K.F. Kelton, J. Chem. Phys. 126 (2007) 054513.
[52] F.A. Çelik, S. Kazanç, *Çankaya University Journal of Science and Engineering* 8 (2011) 63–73.
[53] A. Stukowski, Model. Simul. Mater. Sci. Eng. 18 (2010) 015012.
[54] F. Ding, K. Bolton, A. Rosen, Eur. Phys. J. D 34 (2005) 275–277.
[55] Z. Yang, X. Yang, Z. Xu, J. Phys. Chem. C 112 (2008) 4937–4947.
[56] http://matdl.org/matdlwiki/index.php/softmatter:Mean_Squared_Displacement.
[57] http://www.etomica.org/app/modules/sites/Ljmd/Background2.html.
[58] http://isaacs.sourceforge.net/phys/msd.html.
[59] L. Wei-Zhang, C. Cong, Y. Jian, Heat Trans. Asian Res. 37 (2008) 86–93.
[60] S.Ö. Kart, M. Tomak, M. Uludoğan, T. Çağın, J. Non-Cryst. Solids 337 (2004) 101–108.
[61] H.H. Kart, M. Uludogan, T. Cagin, M. Tomak, J. Non-Cryst. Solids 342 (2004) 6–11.
[62] T. Iiada, R.I.L. Guthrie, The Physical Properties of Liquid Metals, Clarendon, Oxford, 1988.